SAN FRANCISCO BAY
NUTRIENT MANAGEMENT STRATEGY

Long-term Forcings: Generating and searching for trends in a whole-bay remote sensed turbidity record from 2002-present

Contributors:
Daniel Killam[1], David Senn[1], Lindsey Sim[1]

Technical Contributors:
Raphe Kudela[2], Richard Stumpf[3], Shelly Tomlinson[3], Andrew Meredith[3], Brian Bergamaschi[4], Tamara Kraus[4], Katy O'Donnell[4]

[1]San Francisco Estuary Institute; UCSC[2]; NOAA[3]; USGS[4]

July 2026
SFEI Contribution #1277

ACKNOWLEDGEMENTS

This work was funded by the San Francisco Bay Nutrient Management Strategy and the United States Environmental Protection Agency (Agreement# W9-98T54801-0, Destination Clean Bay).

This project has been funded wholly or in part by the United States Environmental Protection Agency under assistance agreement W9-98T54801-0 to the San Francisco Estuary Institute. The contents of this document do not necessarily reflect the views and policies of the Environmental Protection Agency, nor does the Environmental Protection Agency endorse trade names or recommend the use of commercial products mentioned in this document, as well as any images, video, text, or other content created by generative artificial intelligence tools, nor does any such content necessarily reflect the views and policies of the Environmental Protection Agency.

1 PLAIN TEXT SUMMARY

This project represents the first effort to use satellite data to create a long-term, multi-satellite San Francisco Bay-specific turbidity dataset. Having accurate turbidity data will ultimately improve estimates of long-term gross primary productivity, and allow quantification of long-term trends in phytoplankton production. While some measurements of long-term turbidity in San Francisco Bay (SFB) are available from SFEI moored and mapping monitoring, USGS Peterson cruises, USGS sondes, and other sources, there are significant spatial and temporal gaps in the data. The spatial gaps include marginal habitats such as the South Bay shoals and shallow regions of San Pablo Bay–regions' whose wide expanses and variable turbidity are important in determining bay-wide phytoplankton production. Satellite remote sensing is a natural fit for addressing this need, and this work used Sentinel-3 data collected approximately every two days from 2016 to present and MERIS data from 2002-2012 to begin assembling a turbidity dataset. Combining data from the two satellites required extensive testing and refinement, which included converting pixel values to units of turbidity (Formazin Nephelometric Units, FNU), identifying the appropriate spectrometric bands and atmospheric corrections, removing shallow areas that were subject to reflectivity-related interference, correcting for cloud shadows, and validation using data from moored sensor stations and cruises. The result of these efforts is a single, continuous turbidity dataset from 2002 to present, the first such application to SFB. While the data may currently miss some of the high FNU values observed in-situ samples, generally, the surface FNU values calculated from the remote sensed values are representative of expected conditions. Based on a preliminary assessment of the dataset, turbidity appears to be stable but highly variable at the San Pablo Bay region, while the South Bay shows a comparative decline in year-to-year variability. The Lower South Bay also shows increasing turbidity from 2016 onward. This work also assessed the influence of wind and tide, finding that both wind and tidal velocity generally increase observed turbidity in the shallow South Bay shoals. High tide tends to moderate and reduce observed turbidity, likely by reducing wind-based entrainment and encouraging settling. Future work will try to disentangle what trends in the record were caused specifically by wind or tide changes, and whether additional forcings can be integrated into the model.

2 OBJECTIVE/RATIONALE

Our objective is to create a whole bay record of remote-sensed turbidity data in Formazin Nephelometric Units (FNU), to use in investigating multidecadal and shorter-term trends in turbidity. This turbidity field would also be useful for calculation of light attenuation conditions in waters throughout the Bay, for use in biogeochemical modeling, which in the case of our team has previously relied on interpolation approaches.

While long-term measurements of sediment supply are available, to confidently estimate long-term trends, there is still a need for spatially-resolved and temporally consistent measurements of turbidity with consistent periodicity and even spatial sampling back in time. This is particularly in marginal environments where collection is sparser, such as the South Bay shoals, shallow regions of San Pablo Bay, and other similar localities. These locations are generally less accessible for boat-based monitoring compared to the better-studied channel, yet the variability of turbidity of these shallow regions in terms of turbidity can be much greater due to tidal and wind-driven factors.

Satellite remote sensing is a natural fit for such applications, with twin Sentinel-3 satellites collecting data every day on average back to 2016, and before that, a similar satellite, MERIS, collecting similar data from 2002-2012. An algorithm converting the spectrometry products from each satellite to turbidity in estuarine environments is available, from Nechad et al. 2010, but this algorithm has never been applied or vetted in the San Francisco Bay and Estuary, and never compared between the two satellite systems to create a combined record of estuarine turbidity.

3 INTRODUCTION

San Francisco Bay (SFB), despite being nutrient-enriched compared to many estuaries, has historically been considered resistant to elevated production and eutrophication. One factor that has contributed to SFB's relatively low productivity is high suspended sediment concentrations, which reduce photic depths and therefore suppress photosynthesis by phytoplankton. Light attenuation, which can be calculated as a function of turbidity and/or suspended sediment concentration (SSC), is an important parameter in calculations of Gross Primary Production (GPP) in estuaries (Cloern et al. 1995). We set out to investigate long-term trends in Baywide and regional turbidity through time, which would have implications for future management decisions regarding production in SF Bay.

Remote sensed spectrometry has long been used to estimate concentrations of suspended materials in marine environments, including in SF Bay including chlorophyll-a (Kudela et al. 2024), and Suspended Particulate Matter (Taylor et al. 2021). More recently, satellite radiometry has been used to estimate turbidity in estuarine environments in terms of Formazin Nephelometric Units (FNU) (Nechad et al. 2010). Such approaches generally require specific calibration to each individual estuary for each satellite instrument, since sediment composition, tidal and atmospheric conditions differ greatly between estuaries. Previous investigations have used various satellite spectrometry datasets, including ENVISAT MERIS (active from 2002-2012) and Sentinel-3 Ocean and Land Colour Instrument (OLCI) (2015-present) datasets, which each have 300 m resolution and the spectral bands necessary for turbidity reconstruction (Dogliotti et al. 2015). Such data can be used to validate other bands for use in a combined record from 2002-2012 and 2015-present, bridging the MERIS and OLCI satellite datasets, by calibrating the remote sensed data based on ground observations. Despite having comparable spectral and radiometric resolution, the datasets are rarely used in unified long-term biogeochemical trend investigation, and never for estimation of turbidity.

As part of this work, we seek to reconcile and produce a combined long-term record of turbidity applicable to San Francisco Bay, then turning to investigating regional and Baywide trends in turbidity from 2002-present. We then use the approach of Beck et al., 2022 to investigate multiyear variability over different subembayments of SFB, and also compare to coeval wind and tide data to investigate the different sources of variability responsible for sediment resuspension in different regions of SFB.

4 METHODS

MERIS ENVISAT and Sentinel-3A and B OLCI radiometric data were downloaded for the duration of each dataset, with particular focus on the red-edge bands at RRS 665 nm and RRS 709 nm. The satellites flew over SF Bay approximately every two days for MERIS and daily for OLCI, resulting in 3724 data points (1209 for MERIS and 2515 for OLCI), arriving over SF Bay generally between the hours of 9 am and 12 pm Pacific Standard Time (Fig. 1) and transiting in about 3 minutes. Raw spectral data were atmospherically corrected, cloud and land masked, and reprojected to the UTM 10N WGS 84 map projection and saved as .img files for investigation. Water-leaving reflectances were converted to FNU based on the approach of Nechad et al., 2010. RRS665 and 709 are commonly used bands for reconstruction of turbidity in moderately to highly turbid estuarine and marine settings (Sokoletsky et al. 2012; Neil et al. 2011; Chowdhury et al. 2023; Binding et al. 2005), and our validation approach set out to compare the bands and their performance with MERIS and OLCI data, and also to assess the effects of different atmospheric corrections, including C2RCC, used for the OLCI data, and FUB-CSIRO, used for MERIS. Bathymetry data was downloaded from the California Natural Resources Agency in the form of a 10-meter Dynamic Elevation Model (version 4.1, December 2018). The DEM was used to select a region 0.5 m above Mean Low Low Water (MLLW). This area was treated as frequently exposed in the dataset, and used to generate a mask for the remote sensed data excluding the shallowest areas of the Bay such as salt ponds and mud flats which could be more inclined to reflectivity-related interference (Saylam et al. 2017). Because SF Bay is frequently covered by patchy banks of clouds, which often produce horizontally extended shadows in the morning hours, the IDEPIX pixel classification tool for SNAP was used to assist in masking out cloud shadows, which could otherwise lead to reduced FNU estimates.

Figure 1: Times of Sentinel (split into twin S3A and S3B satellites) and ENVISAT MERIS satellite flyovers (Pacific Standard Time). Spikes in recorded S3A times are due to sometimes 15-minute resolution of reported flyover times in the metadata.

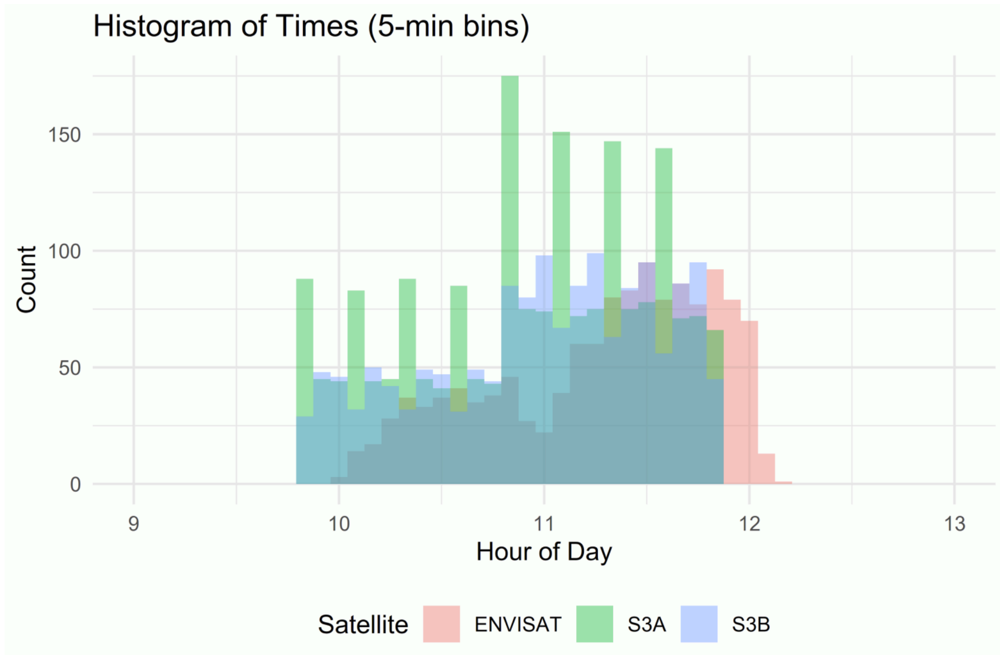

The validation datasets included a selection of thirteen long-term suspended sediment moored monitoring stations maintained by US Geological Survey (Fig. 2), and turbidity data from high-frequency mapping cruises conducted by SFEI in partnership with USGS (Fig. 3). SSC and turbidity data was downloaded from NWIS, at each station from the shallowest available sensor. The suspended sediment stations vary in the start and end dates (Table 1). While stations are reported on the USGS site in SSC (mg/L), the YSI or DTS sondes at the different stations also include turbidity data, and any missing raw turbidity data was back-calculated based on annualized regression relationships reported by USGS (Rasmussen et al. 2009). Data was also excluded based on low quality control scores reported in USGS data. The result is over 20,600,000 entries of fifteen-minute data across the different sites. Satellite data were matched to direct mooring observations based on medians within a 300 m radial buffer around each mooring, with medians, maximum/minimum and pixel counts recorded for each region. Those values were then matched to the mooring data based on the closest 15-minute data point in the moored dataset.

Figure 2: Map of USGS turbidity stations used in this study

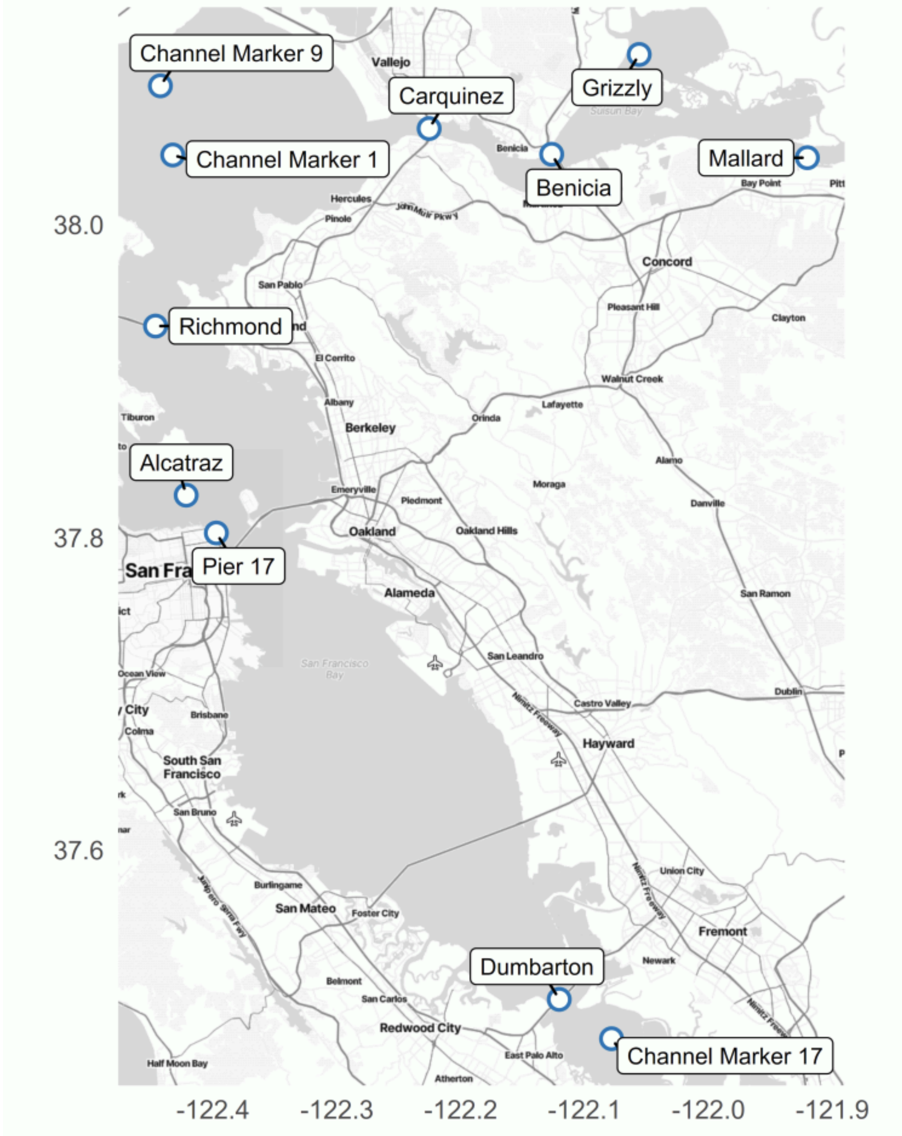

High-frequency mapping validation data represents 43 cruises collected between 2021 and present, from a region extending from Suisun Bay and Rio Vista to the mouth of Lower South Bay past the Dumbarton Bridge (Fig. 3). Turbidity ranges from 1.5 to 382 FNU, with the highest values observed in the San Pablo Bay shoals, Suisun Bay, South Bay Shoals, and Lower South Bay. YSI EXO sondes were set to record results in FNU every second, resulting in over 1,088,000 data points across the dataset. Satellite data were matched to mapping observations based on exact match between the pixel coordinate and mapping coordinate, for cruises on the same day. Mapping observations were transformed by a 3-minute moving average, which assuming a 10 m/s average ship speed would translate to averaging over 1.8 km of ship transit. Points were also delineated by time difference in hours from the satellite flyover. Values were then cross-plotted for comparison to assess the degree of covariation in the satellite and direct observed data.

Table 1: Start and end dates of various USGS turbidity records, and depth of sensors where noted.

Station	Start	End	Depth (m below MLLW)
Alcatraz	2003-11-06	2025-10-08	1.6
Alviso	2010-10-14	2017-06-06	surface
Benicia	2001-05-01	2025-10-08	3.3
Carquinez	2021-08-05	2025-10-04	surface
Channel Marker 1	2003-10-28	2005-10-21	
Channel Marker 17	2003-12-02	2005-04-20	
Channel Marker 9	2002-02-25	2005-10-21	
Dumbarton	2011-10-13	2025-10-08	6.1
Grizzly	2018-01-01	2025-10-01	surface
Mallard	2003-12-10	2025-10-08	1
Pier 17	2018-01-01	2025-10-08	3.7
Richmond	2006-10-18	2025-10-08	12.2

Time series analyses of the resulting satellite data were also conducted. Data were aggregated according to a custom grid integrating different regions across SF Bay, seeking to delineate channel and shoal related areas (Fig. 4). The medians, maximum, minimum, and pixel counts of each parcel were then extracted across the MERIS and OLCI datasets. Long-term trends were extracted from the data via the moving window Generalized Additive Model approach outlined in Beck et al., 2022, producing trend estimates throughout the combined 2002-present record.

Additional Generalized Additive Models were generated comparing the values of polygons to coincidently collected wind and tide data, to investigate the correspondence of turbidity with known sources of resuspension. 6-minute wind data from 2005-2024 was obtained from NOAA National Buoy Data Center Center station 46026 (Alameda), along with 15-minute tide data from NOAA tide station 9414750 (Alameda). 24-hour right aligned moving average windspeed and tide level were compared to parcel averages with a Generalized Additive Model following the formula:

FNU ~ s(D, knots=200) + s(H) + s(W) + s(V)

Where D is decimal year, H is tide stage in meters, W is 24-hour moving average wind speed in m/s, and V is instantaneous tidal velocity in m/hr.

Figure 3: High frequency mapping cruise turbidity observations. Values range from 0 to 160 FNU. 43 cruises are available for comparison to Sentinel-3 data.

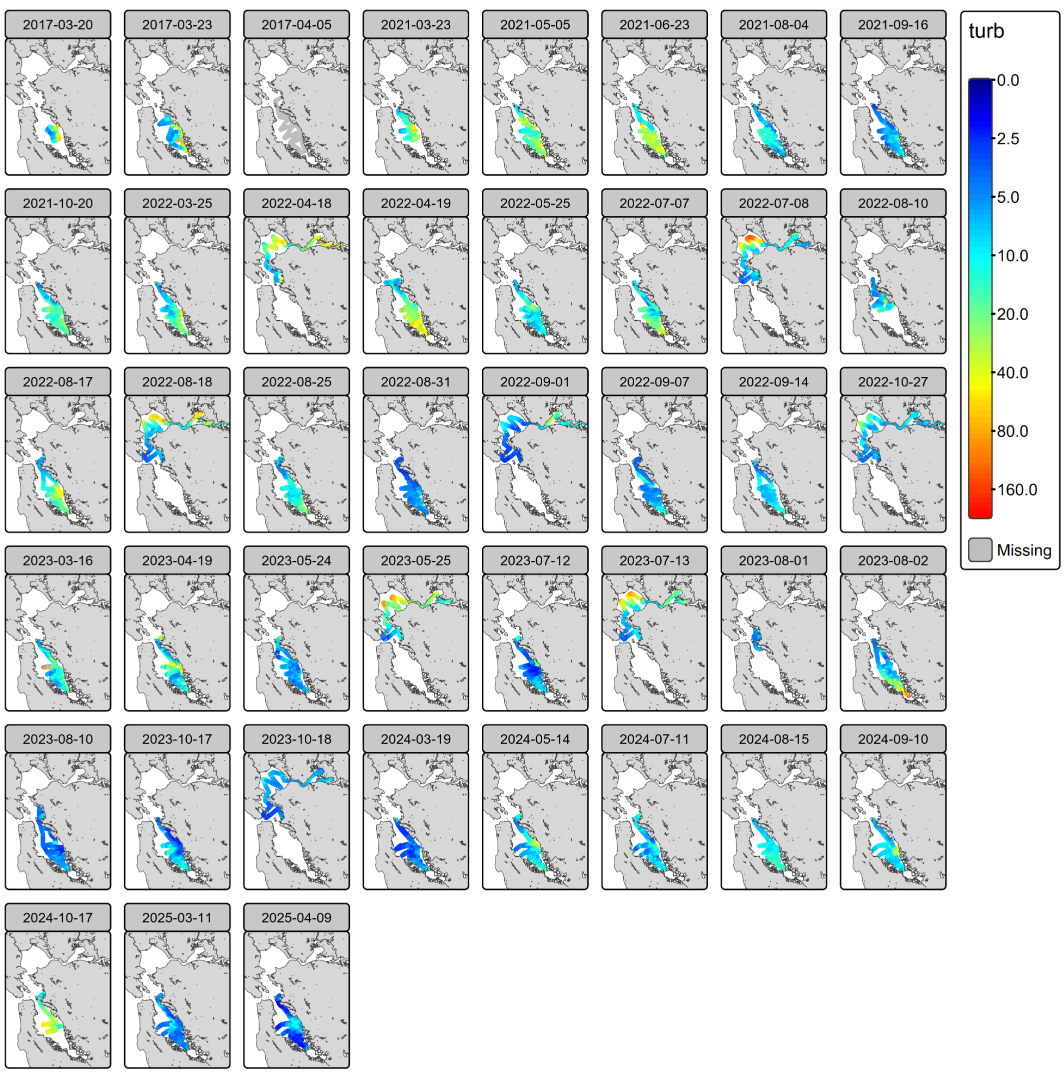

Figure 4: Regions averaged over for time series analysis. Names and colors are used in some visualizations below.

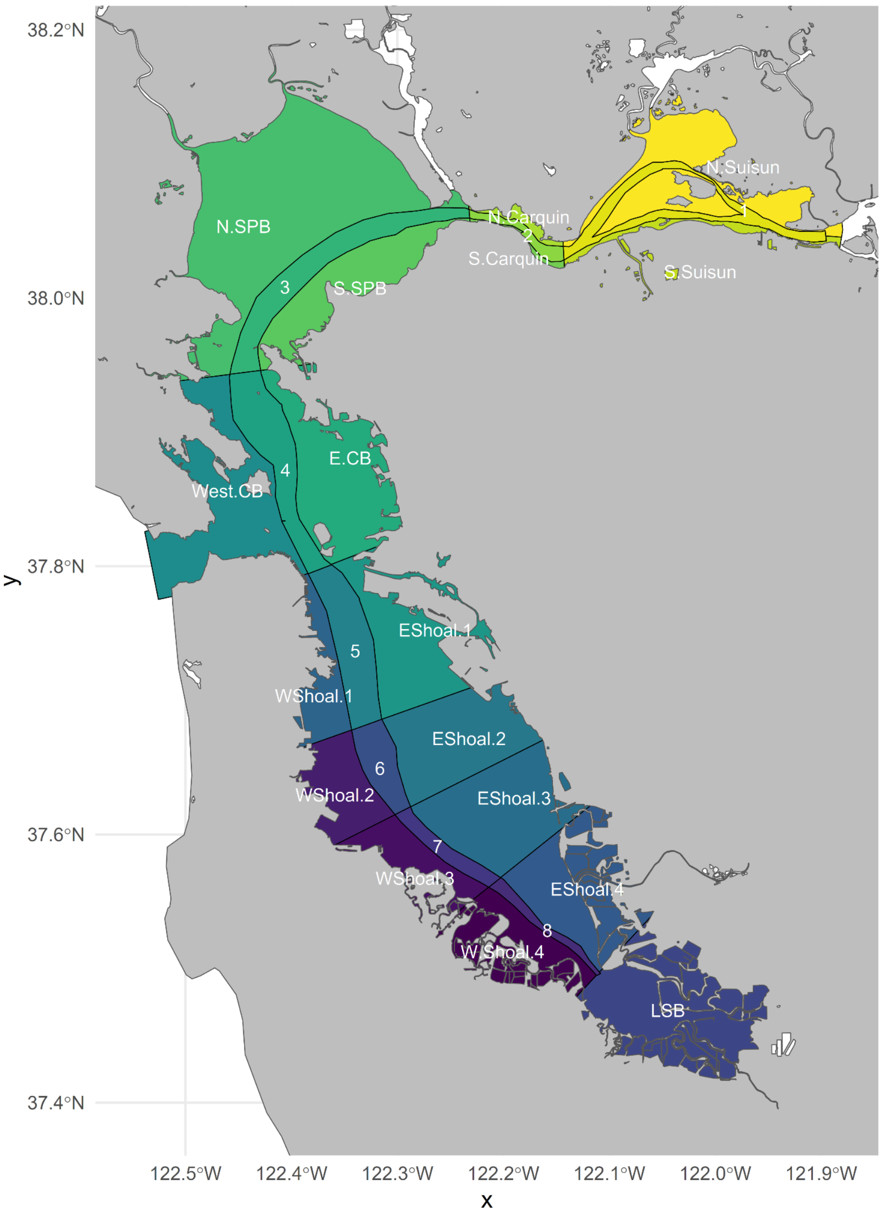

5 RESULTS AND DISCUSSION

5.1 Validation

The FUB-CSIRO atmospheric correction was found to be the most effective with MERIS data (Schroeder [2022] 2024), as the C2RCC correction caused issues regarding exclusion of Suisun Bay in that dataset, potentially due to reflectivity of that water body at the time of day transited by the satellite. C2RCC was used for the OLCI-originating data (Brockmann et al. 2016). The RRS 709 band was found most effective at resolving the entire range of expected turbidity values, particularly in San Pablo and Suisun Bays, where the RRS 665 band produced results mostly capped at 20 FNU for MERIS data, while prior observations of those areas had found SSC/turbidity values frequently exceed those amounts (Fig. 3, 5) (Schoellhamer 2011; Cloern and Jassby 2012). Particular care must be given to choosing and parameterizing the atmospheric correction for each instrument, as the single-band algorithm used is highly sensitive to minor changes in output surface reflectance, even among comparable sensors between MERIS and OLCI.

Figure 5: Left: Histogram comparing RRS 665 to RRS 709 observed FNU values for a MERIS observation from 2004-06-28. RRS 665 records no values above 20 FNU, while 709 has a broader distribution extending above 30 FNU. Right: Map showing that flyover day, comparing calculated values of 665 subtracted from 709. 665 frequently underestimates FNU from shallow marginal environments such as the San Pablo Bay shoals, Grizzly Bay and parts of Lower South Bay.

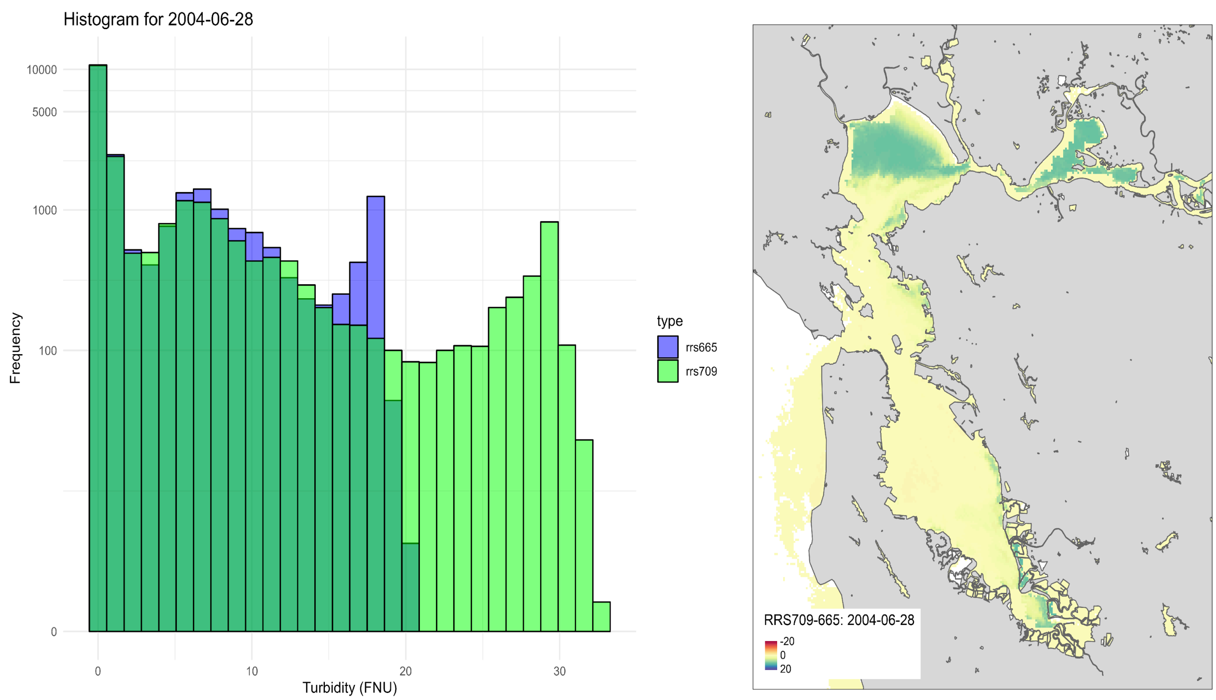

Cross-plotting MERIS and OLCI data with concurrent direct turbidity observations from the USGS sonde network, we find linear relationships (in log-10 space) between remote-sensed and mooring-observed FNU values (Fig. 6). At some stations the relationships are close to 1:1, such as Mallard, Benicia, and Grizzly, while others may have slight satellite underestimates of turbidity at the high end of the distribution around 100 FNU, such as Dumbarton, Richmond and Carquinez. The Alcatraz station shows the greatest deviation from the 1:1 relationship for both the MERIS and OLCI satellite eras, with those residuals resulting primarily from FNU underestimates from the satellite. Mallard, Benicia and Grizzly Bay are shallower sites where the correspondence between satellite observations (generally restricted to the surface layer) is expected to be closest. The

Alcatraz station as well as the bridge stations (Dumbarton, Richmond, and Carquinez) are in deeper subembayments or along the Bay channel where the sensor could be 20-40 feet underwater depending on tide stage. This may produce deviations between surface-observed values and sonde-measured turbidity at depth due to the settling of particles, leading to the satellite observing less turbidity than is seen by the sonde at depth. The settling velocity is expected to be greater in deeper areas of estuaries, where tidal and wind-driven suspension are reduced (Uncles et al. 2002).

Figure 6: Crossplots comparing remote sensed FNU values to observations from the USGS sediment monitoring network. Data is subset to compare versus Meris and Sentinel-3 data

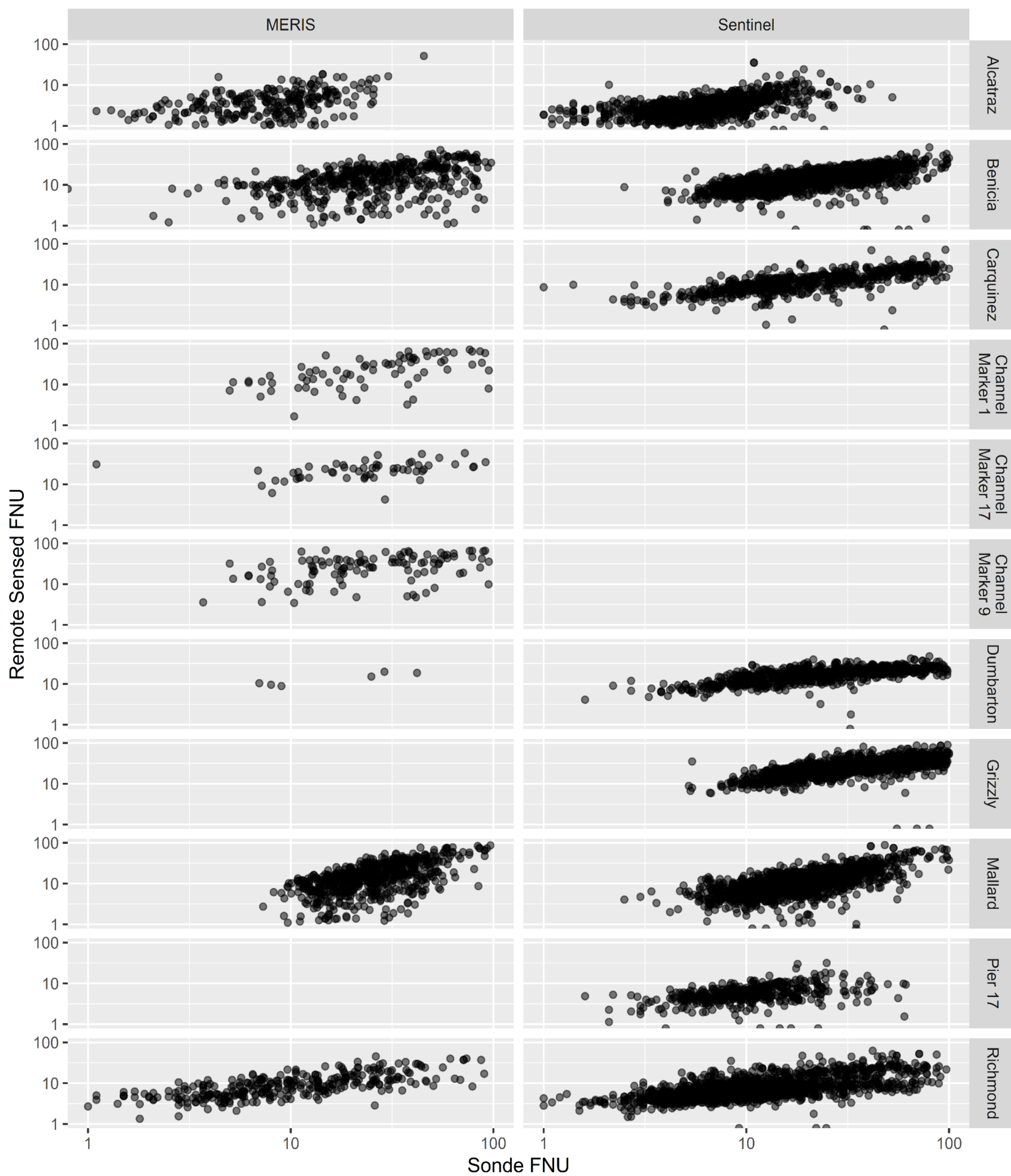

Most of the publicly available data from USGS stations does not include depth measurements. However, in future analyses, approximate sensor depth can be reconstructed by combining the USGS-reported depth from bottom with the known tide stage, recorded by NOAA-maintained sensors throughout the Bay. This would allow for the validation dataset to be subset, and a combined model incorporating sensor depth could be used to compare satellite values to turbidity values at the sensor depth. Such a model could be used to search for tidal and seasonal trends in surface-bottom divergences in turbidity, and the influence of hydrological processes on particle settling velocity in SFB.

Figure 7: Crossplot comparing cruise-measured FNU values to observations from Sentinel-3

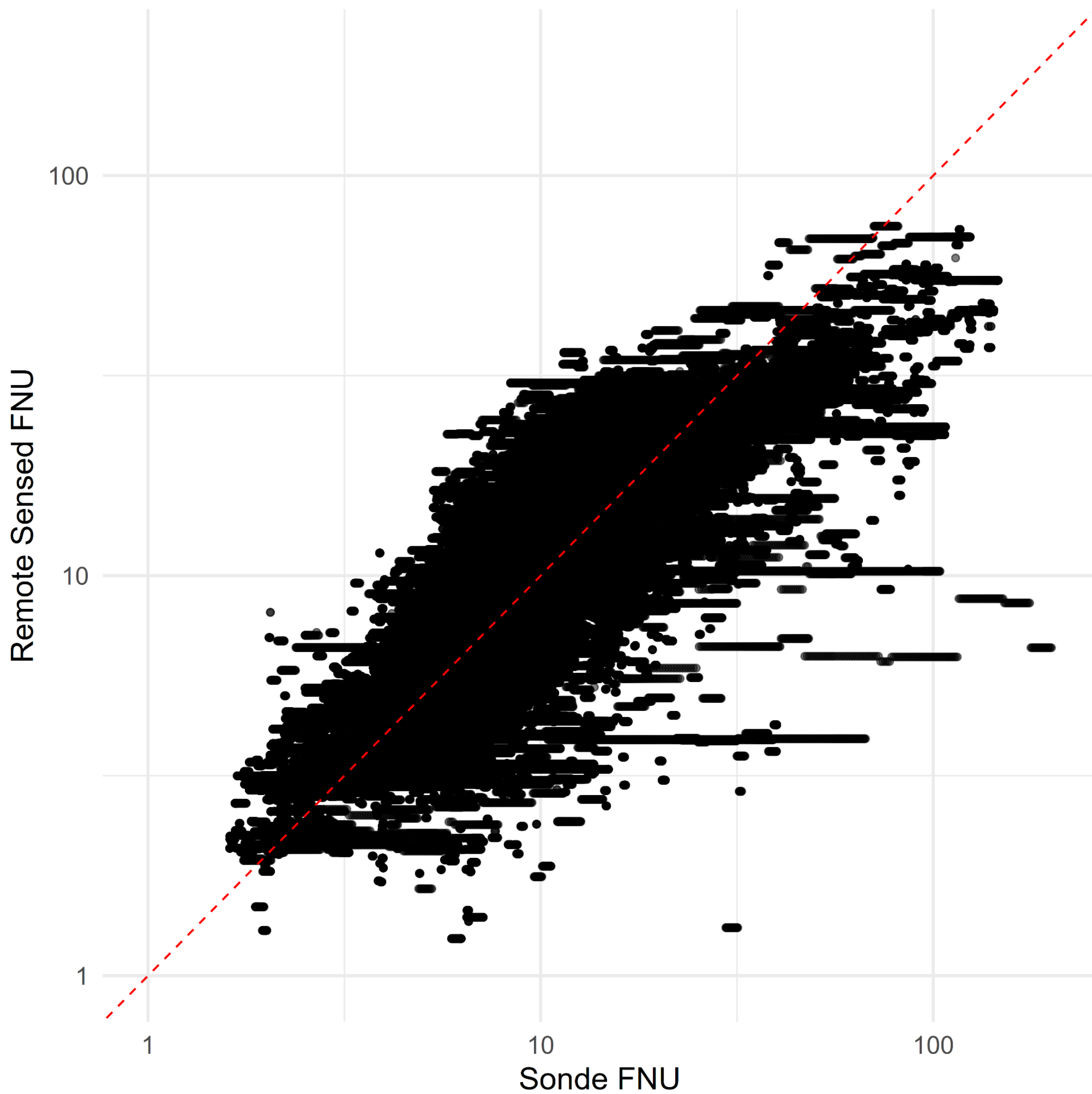

Figure 8: Maps showing residuals of cruise-observed and satellite-measured data. Color represents the remote sensed value minus sonde-observed values. In most cases, the satellite hovers around 0 difference, but there are some instances where the satellite underestimates turbidity, such as 2022-07-08 on the San Pablo Bay shoals.

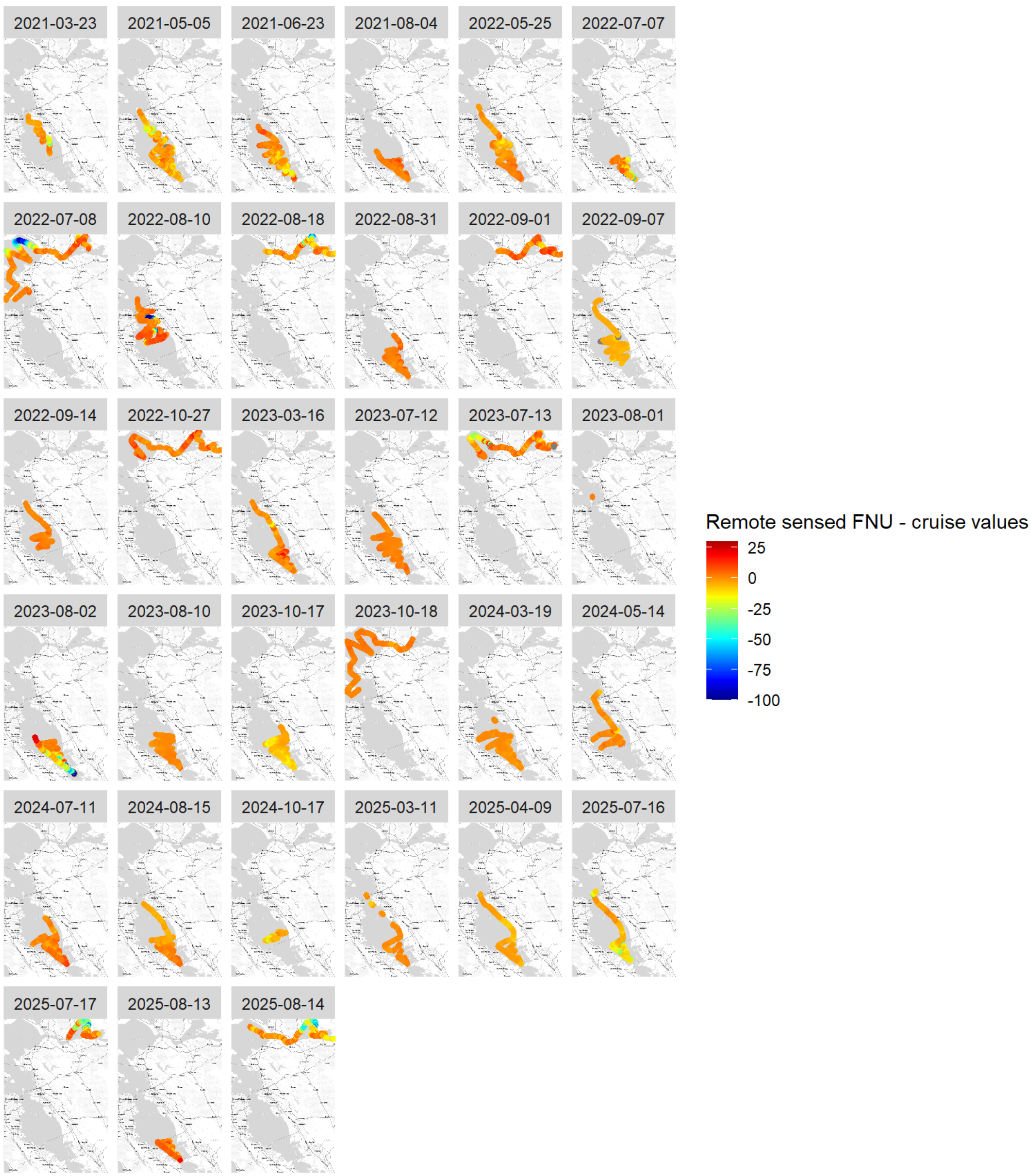

Figure 9: Boxplots showing medians and interquartile ranges for each of the characteristic parcels, arranged approximately in order of turbidity. Colors and names match with the map in Figure 4. A) All MERIS and Sentinel-3 data together. B) MERIS and Sentinel data separated.

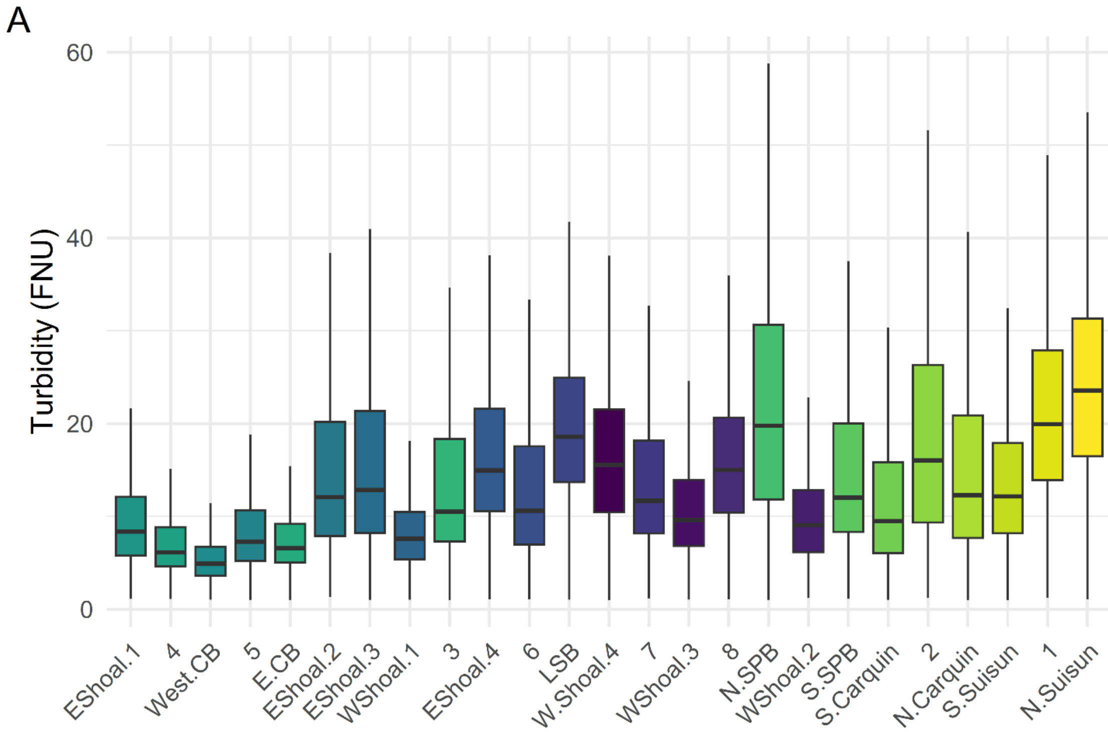

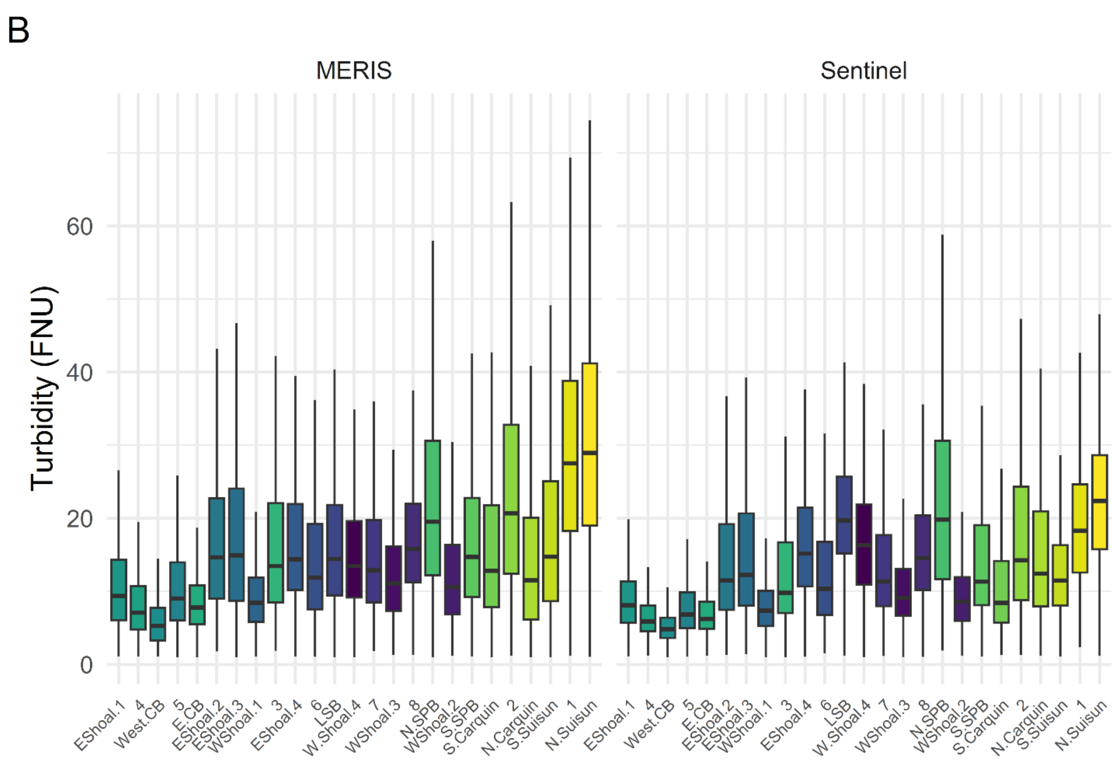

Comparing the high-frequency mapped FNU values to satellite-calculated FNU, we observe that the relationship generally clusters around the 1:1 line throughout the distribution, with residuals increasing in relative size at higher FNU values, and a tendency towards slight underestimates at the highest FNU values observed by the mapping cruises (Fig. 7). Because these comparisons are all at the surface, unlike the mooring validation dataset, it is probable that the underestimation of FNU by the satellite is due to the spatial averaging associated with the 300 m pixel size from the satellite. Previous investigations have determined with highly variable, "spiky" data like turbidity or SSC, coarser sampling resolution associated with remote sensing generally reduces observed maxima by averaging results over a broader area (Dorji and Fearns 2017). While in our cross-comparison we averaged over 3 minutes of cruise observations, future validation work may benefit from binding mapping data to the satellite spatial grid and averaging results spatially instead.

In the comparison of high-frequency mapping data, the results do not generally seem biased towards higher or lower in any particular subembayment, with most satellite results falling within 20 FNU of observations in the positive or negative directions (Fig. 8).Three pronounced deviations can be observed, with direct ship measurements much higher than those reconstructed by the satellite (Fig. 7). On the map, these results correspond to legs of cruises on 2022-07-08, 2023-08-02, and two cruises in 2025, when the ship passed into shallow areas including San Pablo Bay, Lower South Bay and Grizzly Bay (Fig. 8). In each case, the satellite recorded values lower than that observed from the ship, and passed over before the ship reached that respective location. This suggests wind or tide-driven resuspension during the interval between the satellite and ship recording turbidity at that location. Future comparisons can investigate the degree to which the closeness of temporal match influences such deviations between satellite and directly observed data, since turbidity is quite temporally variable in times of high winds or tidal velocity.

5.2 Spatial variability and differences between the datasets

Medians of characteristic regions across MERIS data from 2002-2012 and OLCI data from 2016-present show generally similar spatial patterns (Fig. 9). Suisun Bay shows the highest FNU values, approaching 30 FNU, and a large interquartile range, while the Central Bay is generally lowest, with median values below 10 FNU. Other shallower areas of the Bay also show elevated turbidity medians, such as the northern area of San Pablo Bay, and parts of the South Bay shoals. Both the eastern and western shoals of the South Bay show higher turbidity than the channel, and there is a gradually increasing North-South trend in South Bay approaching the Dumbarton Bridge. Between the datasets, Lower South Bay has a median of 20 FNU in OLCI data, and only 15 FNU in the MERIS dataset, while Suisun Bay shows the opposite pattern, with the MERIS dataset showing a median almost 10 FNU higher than is present in the OLCI data.

Generally, the two satellites record similar overall spatial patterns, when plotting medians across the entire respective MERIS and OLCI datasets (Fig. 10). Satellite-observed FNU values in the channel are generally lower than the adjacent shallow areas, particularly in the North Bay. But because variance in turbidity in these regions is greater, there are points in the record when the channel records higher FNU values than the shoals. Deeper waters of the channel can display higher FNU values than would be observed by satellites at the surface, with much of that exported turbidity originating from the shoals, resulting from resuspension in those environments (Conomos and Peterson 1977).

Figure 10: Left: median values across the entire MERIS dataset. Right: median across entire Sentinel dataset.

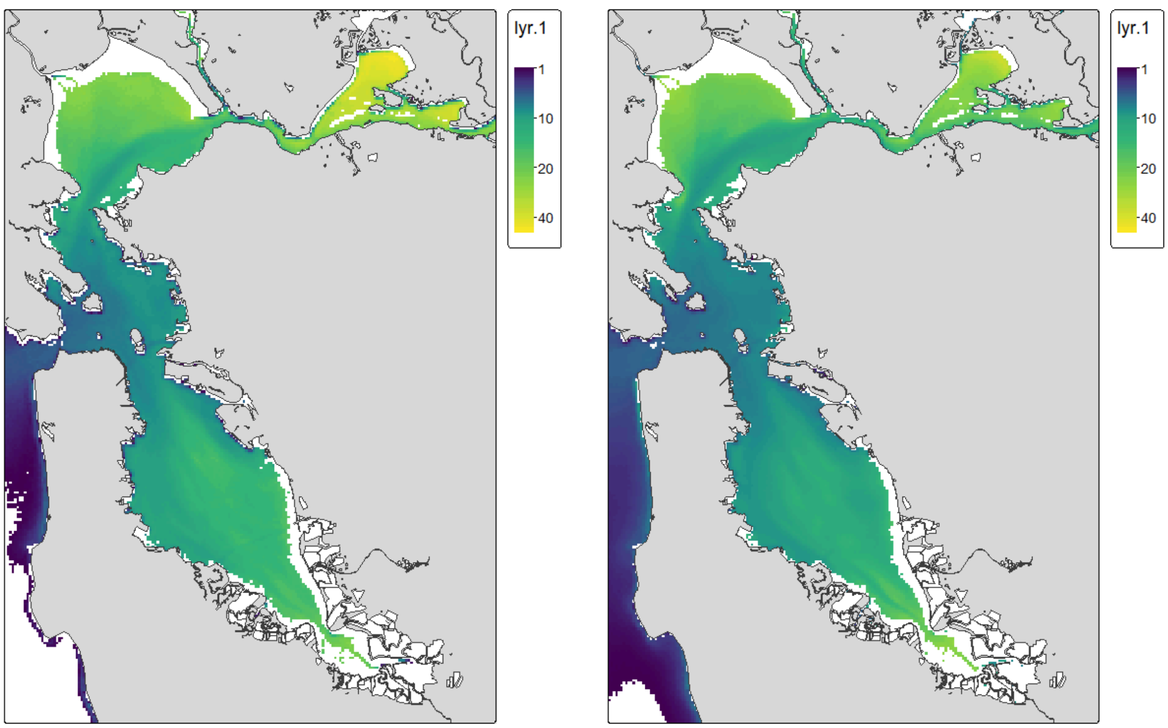

5.3 Variability in FNU through time: Forcings

In the South Bay, the median values across the Western and Eastern shoals and central Channels are broadly similar between the MERIS and OLCI eras (Fig. 11), despite the more frequent sampling in the OLCI years. The Eastern shoals frequently display elevated turbidity conditions in excess of 50 FNU, while those values are more unusual to observe over the channel. The variability in turbidity is also higher over the Eastern shoals compared to the channel, with large swings observed, including increases in the spring aligning with higher wet-season flows (Cloern et al. 1985). The Western shoals tend to covary more closely with the channel values, also showing similar medians as the channel through time. As the narrow western shoals are closely bordered by the channel, it is likely that conditions are more closely coupled to the channel than is seen on the eastern shoals, which have broad shallow regions of greater spatial isolation, and representing more area for variability in wind and tidal resuspension to produce regionally elevated turbidity values.

Investigating the August-October window that has recently been a focus of the NMS program, we find that different subembayments show differing trends (Fig. 12). The shallow portion of San Pablo Bay shows dramatic up and down swings in turbidity through the record. The Eastern shoals and channel of South Bay show decreased variability in the OLCI era compared to MERIS-observed values. The Eastern shoals show greater variance between years compared to the channel, aligning with the previously mentioned observation that shallow environments have greater capacity for variability both in year-to-year and longer term time scales. The Lower South Bay shows an increase in FNU over the record, paralleling trends in SSC observed in recent years at Dumbarton Bridge (Foley et al., 2025).

Comparing median values observed in parcels “EShoal1-4” (Fig. 4) relative to concurrently-observed wind and tide at Alameda, we observe a general tendency towards higher FNU values at times when 2-hour moving average wind values are high and tides are low (Fig. 13). When a thin layer of water is present over the shoals, winds have greater capacity to produce shear events that turn over and resuspend settled particles contributing to turbidity. When the tide is high, the shearing effect of wind is modulated, and resuspension is reduced. When a GAM is constructed relating time, windspeed, tide stage and tide velocity, the model assigns a partial effect of wind speed equating to approximately 5 additional FNU observed per 10 m/s average windspeed (Fig. 14B). Tide stage has a smaller partial effect on FNU, but each additional meter of tide height equates to approximately 3 lower measured median FNU in different shoal parcels (Fig. 14C). This could be a function of the reduced ability of wind to entrain and agitate bottom waters when tide is high, and also a function of increased ability of sediment particles to settle out of the surface layer when water is deeper. Meanwhile, higher tidal velocity acts to increase turbidity. The increase as a function of negative tidal velocity (outgoing tide) is much smaller than positive velocity, which is likely a function of the particles being exported from the shoals during the outgoing tide faster than they can be suspended (Fig. 14D). Each term of the model is statistically significant, with 42.4% of the deviance explained (adjusted R2 = 0.417) (Table 2).

Figure 11: Time series showing median turbidity values from different parcels including the entire western shoals, the South Bay portion of the channel, and the eastern shoals. The red line is a GAM smooth generated by the approach of Beck et al, 2022.

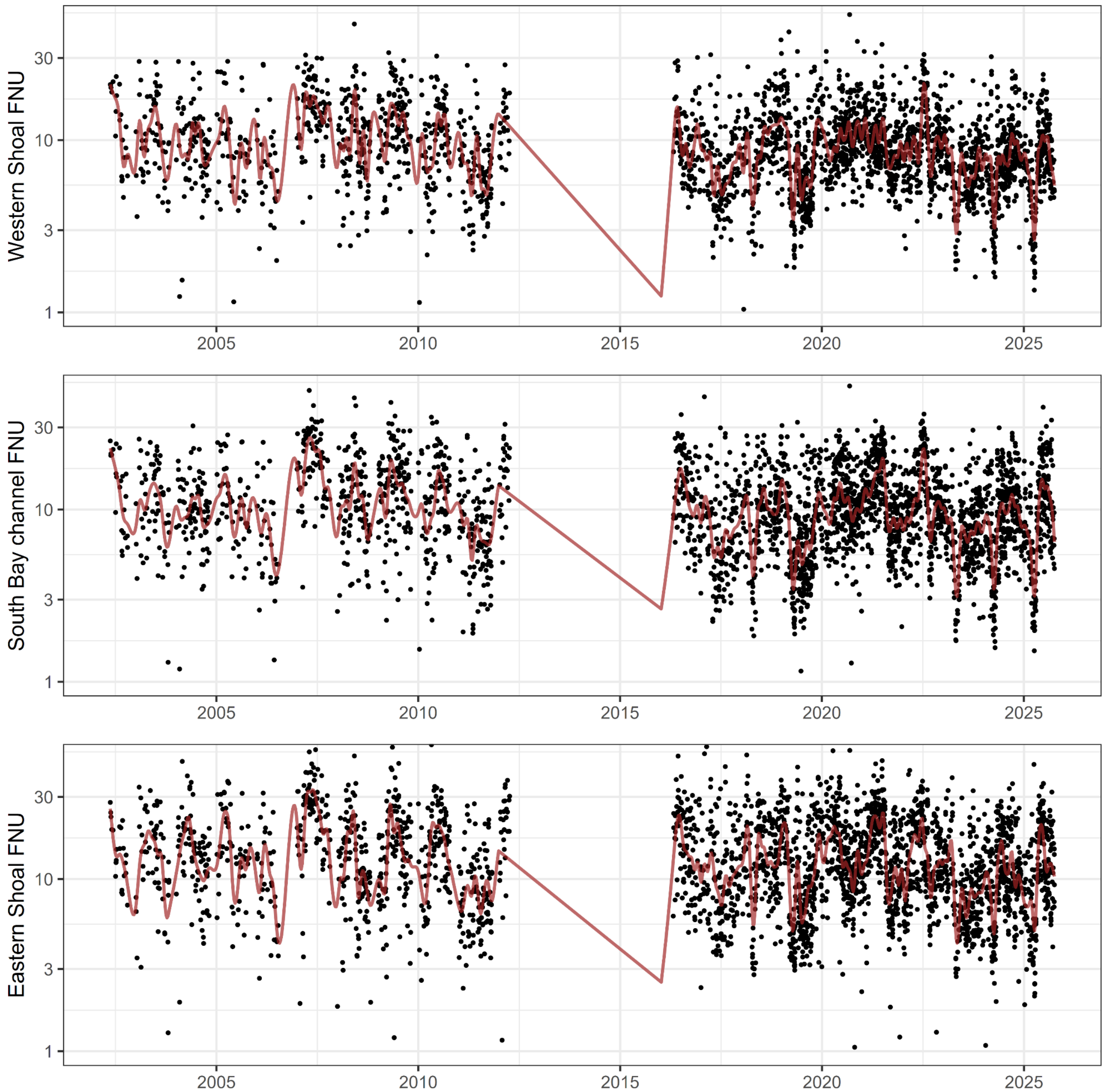

As Fig. 14A shows, there are still sources of interannual variability present in the time series which are not captured by the other terms of the model. Over half of the variability is explained by sources not included in the model. The GAM is based on the year-round data, and there is a possibility that seasonal influxes of turbidity such as from spring flow would help resolve the annual fluctuations. But because satellite coverage can be limited in that season by clouds, care will be needed to ensure that sampling is consistent through the dataset, to adequately measure flow-related forcings relative to the other factors.

Figure 12: Annual medians generated by the approach of Beck et al. 2022, for the August-October window, for different parcels including San Pablo Bay, the South Bay Channel and Shoals, and the Lower South Bay.

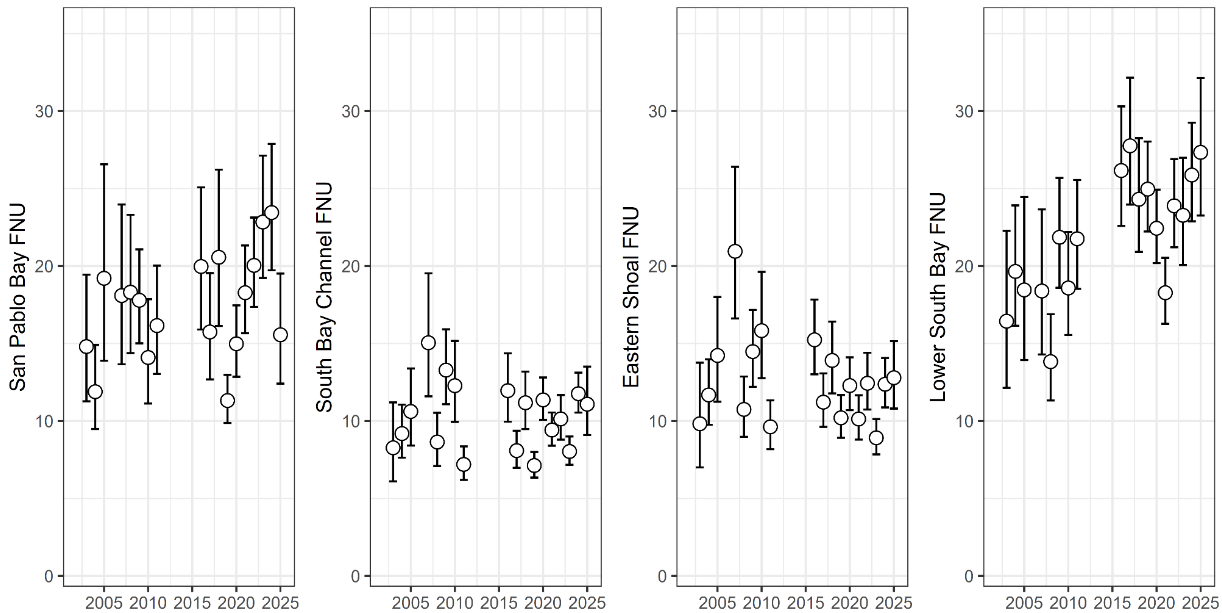

5.4 Conclusion

The combined 2002-2025 satellite record successfully integrates the observations of two satellites, with the outputs of each being intercomparable in terms of observed FNU ranges in different subembayments. The results compared to in situ observations suggest some loss of high FNU values in the satellite data, as a result of either spatial averaging across the 300 m sampling resolution, as well as the impact of particle settling, particularly over deeper water environments such as the Channel and Central Bay. But generally, the surface FNU values calculated from the remote sensed values are representative of conditions expected in San Pablo Bay, Grizzly Bay, the shallowest South Bay shoals, and other regions where in-situ data is comparatively sparse.

In these regions, we can construct models estimating multiyear trends paralleling previous efforts, and also multidimensional models looking at the influence of wind and tide. We found that turbidity appears to be stable but highly variable at the San Pablo Bay region, while South Bay shows a comparative decline in year-to-year variability in the OLCI portion of the record. Lower South Bay shows an increase of turbidity in the OLCI era. Looking at the comparative influence of wind and tide, we find that both wind and tidal velocity exert a positive influence on observed turbidity in the shallow South Bay shoals. High tide tends to moderate and reduce observed FNU due to the twin factors of reducing wind-based entrainment and encouraging settling. Future work will try to disentangle what trends in the record could be forced by wind or tide changes, and whether additional forcings could be integrated into the model, which could in turn be related to trends in biomass, production and other ecological measures of SF Bay long-term health.

Figure 13: Cross-plot comparing 2-hour moving average Alameda wind speed to the tide height at time of satellite transit. Color indicates turbidity values, with yellow corresponding to higher FNU over the South Bay shoals, and purple values indicating low FNU. A) Wind speed vs. tide height. High FNU values generally cluster at times of low tide and high sustained wind speed (top left corner). B) Wind speed vs tidal velocity. High FNU is associated with wind speed, but especially so when coinciding with fastest tidal velocity. Calm days with low wind speed and high tidal velocity are elevated, while calm days with low tidal velocity show lowest FNU values.

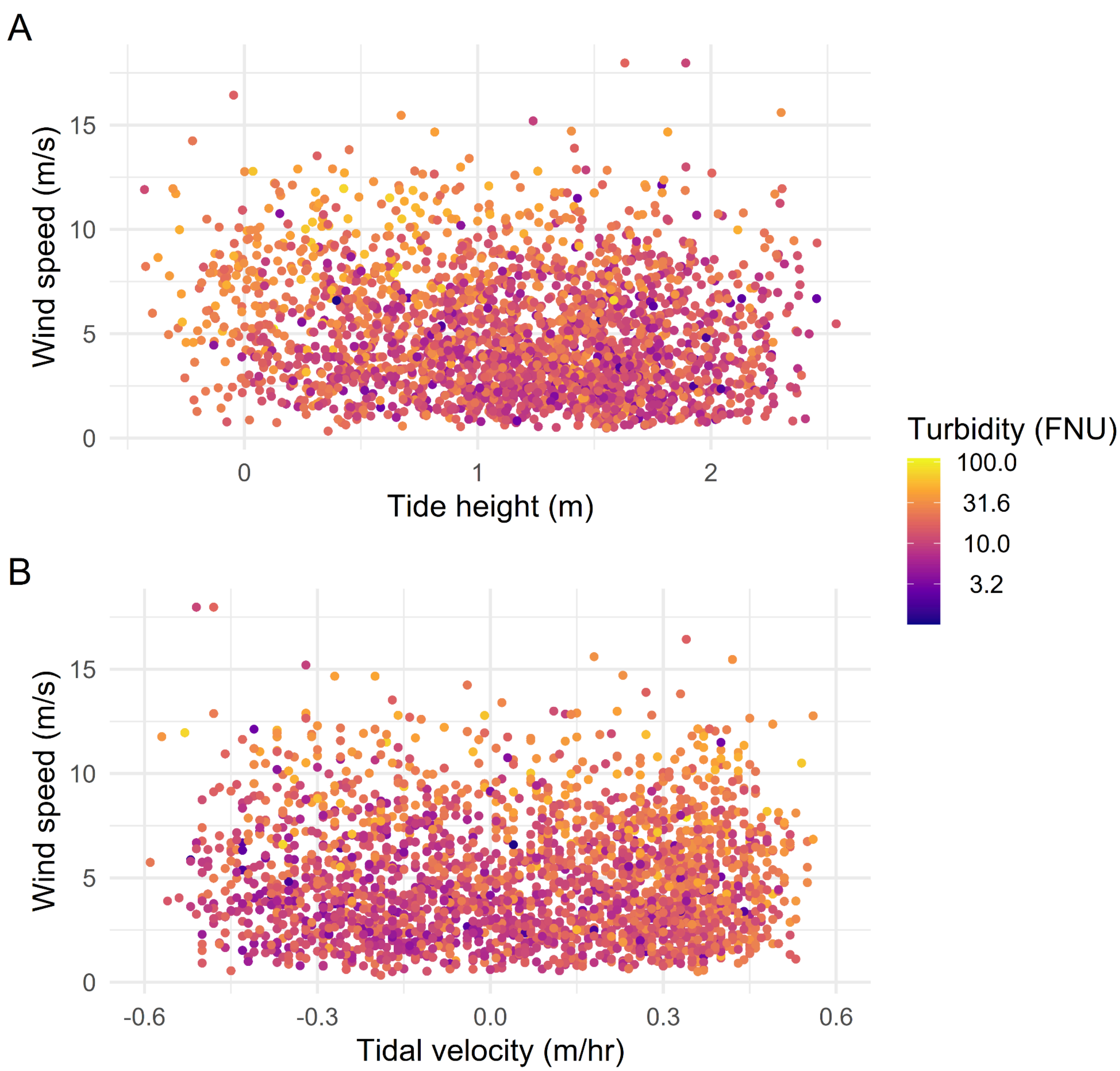

Figure 14: Generalized Additive Model graphs of each term's influence on the South Bay shoal FNU values. A) Showing how decimal year has interannual variability still not captured by the other terms. B) Turbidity increases as a function of wind speed. C) Turbidity declines at higher tide heights. D) Turbidity generally increases at higher tidal velocities, but this relationship is asymmetrical, with positive tidal velocities (rising tide) showing much greater increases in FNU then negative velocities (outgoing tide).

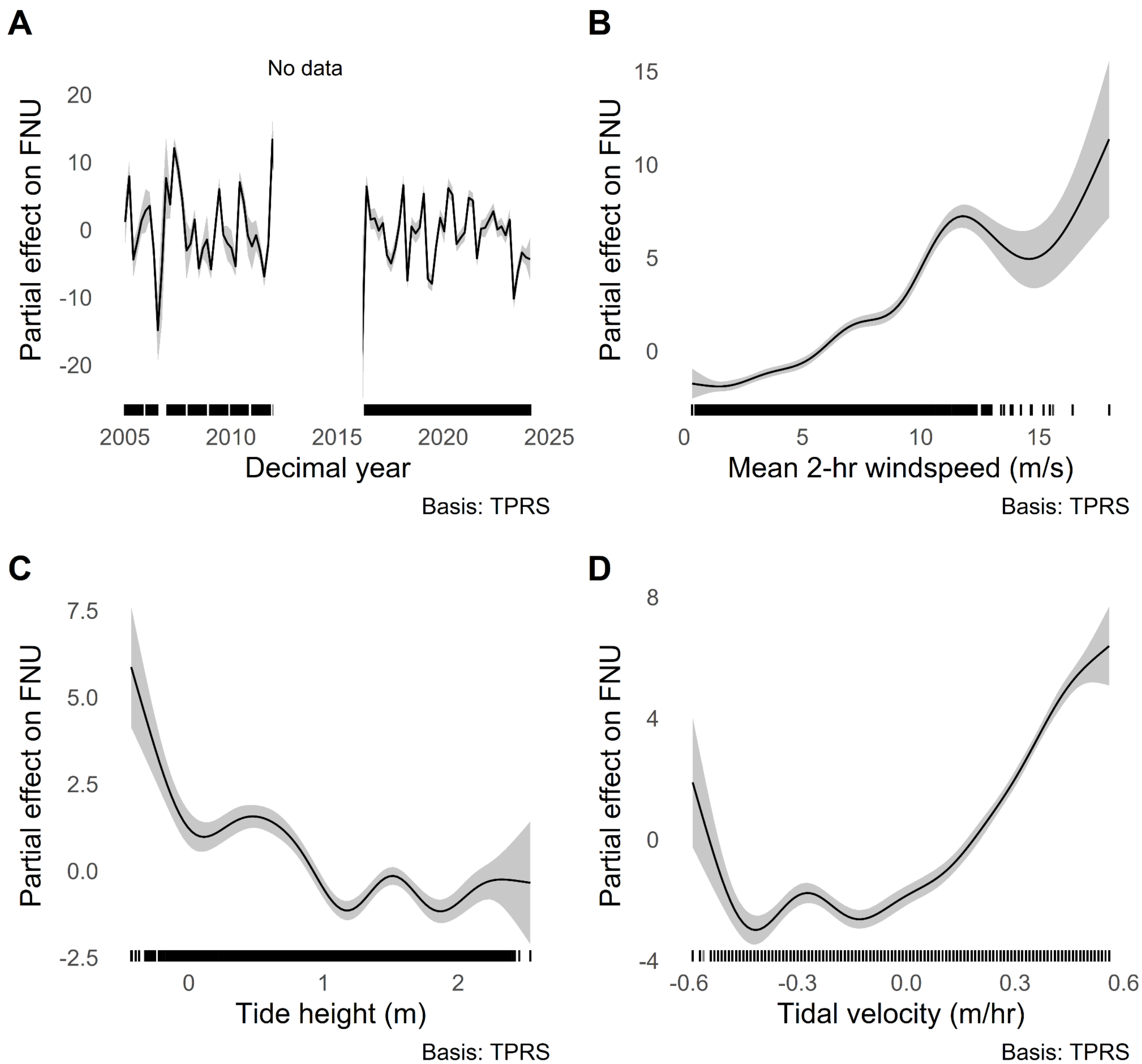

Table 2: Coefficients and errors associated with each term of the GAM.

Term	Estimate	Std.Error	Statistic	p.value
(Intercept)	14.558575	0.05342511	272.50435	p < 0.001 ***
s(decyear)	190.225449	197.94996041	33.59478	p < 0.001 ***
s(TideHT.m)	8.552965	8.94382764	27.34082	p < 0.001 ***
s(spd_mean)	8.703617	8.97251949	141.56440	p < 0.001 ***
s(tidal_velocity)	8.731223	8.97748277	229.57938	p < 0.001 ***

REFERENCES

Beck, M.W., De Valpine, P., Murphy, R., Wren, I., Chelsky, A., Foley, M., Senn, D.B., 2022. Multi-scale trend analysis of water quality using error propagation of generalized additive models. Science of The Total Environment 802, 149927. https://doi.org/10.1016/j.scitotenv.2021.149927

Binding, C. E., D. G. Bowers, and E. G. Mitchelson-Jacob. 2005. "Estimating Suspended Sediment Concentrations from Ocean Colour Measurements in Moderately Turbid Waters; the Impact of Variable Particle Scattering Properties." Remote Sensing of Environment 94 (3): 373–83. https://doi.org/10.1016/j.rse.2004.11.002.

Brockmann, Carsten, Roland Doerffer, Marco Peters, Stelzer Kerstin, Sabine Embacher, and Ana Ruescas. 2016. "Evolution of the C2RCC Neural Network for Sentinel 2 and 3 for the Retrieval of Ocean Colour Products in Normal and Extreme Optically Complex Waters." 740 (August): 54. https://ui.adsabs.harvard.edu/abs/2016ESASP.740E..54B.

Chowdhury, Masuma, César Vilas, Stef van Bergeijk, Gabriel Navarro, Irene Laiz, and Isabel Caballero. 2023. "Monitoring Turbidity in a Highly Variable Estuary Using Sentinel 2-A/B for Ecosystem Management Applications." Frontiers in Marine Science 10 (July). https://doi.org/10.3389/fmars.2023.1186441.

Cloern, James E, Brian E Cole, Raymond LJ Wong, and Andrea E Alpine. 1985. Temporal Dynamics of Estuarine Phytoplankton: A Case Study of San Francisco Bay. Springer.

Cloern, James E., Christian Grenz, and Lisa Vidergar-Lucas Reviewed work(s): 1995. "An Empirical Model of the Phytoplankton Chlorophyll: Carbon Ratio-the Conversion Factor Between Productivity and Growth Rate." Limnology and Oceanography 40 (7): 1313–21.

Cloern, James E., and Alan D. Jassby. 2012. "Drivers of Change in Estuarine-Coastal Ecosystems: Discoveries from Four Decades of Study in San Francisco Bay." Reviews of Geophysics 50 (4). https://doi.org/10.1029/2012RG000397.

Conomos, T. J., and D. H. Peterson. 1977. "Suspended-particle Transport and Circulation in San Francisco Bay: An Overview." In Estuarine Processes, edited by MARTIN WILEY. Academic Press. https://doi.org/10.1016/B978-0-12-751802-2.50014-X.

Dogliotti, A. I., K. G. Ruddick, B. Nechad, D. Doxaran, and E. Knaeps. 2015. "A Single Algorithm to Retrieve Turbidity from Remotely-Sensed Data in All Coastal and Estuarine Waters." Remote Sensing of Environment 156 (January): 157–68. https://doi.org/10.1016/j.rse.2014.09.020.

Dorji, Passang, and Peter Fearns. 2017. “Impact of the Spatial Resolution of Satellite Remote Sensing Sensors in the Quantification of Total Suspended Sediment Concentration: A Case Study in Turbid Waters of Northern Western Australia.” PLOS ONE 12 (4): e0175042. https://doi.org/10.1371/journal.pone.0175042.

Kudela, Raphael, David Senn, Emily Richardson, Keith Bouma-Gregson, Brian Bergamaschi, and Lawrence Sim. 2024. “Evaluation and Refinement of Chlorophyll-a Algorithms for High-Biomass Blooms in San Francisco Bay (USA).” Remote Sensing 16 (March): 1103. https://doi.org/10.3390/rs16061103.

Nechad, B., K.G. Ruddick, and Y. Park. 2010. “Calibration and Validation of a Generic Multisensor Algorithm for Mapping of Total Suspended Matter in Turbid Waters.” Remote Sensing of Environment 114 (4): 854–66. https://doi.org/10.1016/j.rse.2009.11.022.

Neil, Claire, Alex Cunningham, and David McKee. 2011. “Relationships between Suspended Mineral Concentrations and Red-Waveband Reflectances in Moderately Turbid Shelf Seas.” Remote Sensing of Environment 115 (12): 3719–30. https://doi.org/10.1016/j.rse.2011.09.010.

Rasmussen, Patrick P., John R. Gray, G. Douglas Glysson, and Andrew C. Ziegler. 2009. “Guidelines and Procedures for Computing Time-Series Suspended-Sediment Concentrations and Loads from In-Stream Turbidity-Sensor and Streamflow Data.” In Techniques and Methods, Nos. 3-C4. U.S. Geological Survey. https://doi.org/10.3133/tm3C4.

Saylam, Kutalmis, Rebecca A. Brown, and John R. Hupp. 2017. “Assessment of Depth and Turbidity with Airborne Lidar Bathymetry and Multiband Satellite Imagery in Shallow Water Bodies of the Alaskan North Slope.” International Journal of Applied Earth Observation and Geoinformation 58 (June): 191–200. https://doi.org/10.1016/j.jag.2017.02.012.

Schoellhamer, David H. 2011. “Sudden Clearing of Estuarine Waters upon Crossing the Threshold from Transport to Supply Regulation of Sediment Transport as an Erodible Sediment Pool Is Depleted: San Francisco Bay, 1999.” Estuaries and Coasts 34 (5): 885–99. https://doi.org/10.1007/s12237-011-9382-x.

Schroeder, Michael Schaale / Thomas. (2022) 2024. S3tbx-Fub-Csiro/S3tbx-Fub-Csiro. January 15, released December 27. https://github.com/s3tbx-fub-csiro/s3tbx-fub-csiro.

Sokoletsky, Leonid G., Ross S. Lunetta, Michael S. Wetz, and Hans W. Paerl. 2012. “Assessment of the Water Quality Components in Turbid Estuarine Waters Based on Radiative Transfer Approximations.” Israel Journal of Plant Sciences 60 (1–2): 209–29. https://doi.org/10.1560/IJPS.60.1-2.209.

Taylor, Niky C., Raphael M. Kudela, Niky C. Taylor, and Raphael M. Kudela. 2021. “Spatial Variability of Suspended Sediments in San Francisco Bay, California.” Remote Sensing 13 (22). https://doi.org/10.3390/rs13224625.

Uncles, R. J., J. A. Stephens, and R. E. Smith. 2002. “The Dependence of Estuarine Turbidity on Tidal Intrusion Length, Tidal Range and Residence Time.” Continental Shelf Research, Proceedings from the Tenth Biennial Conference on the Physics of Estuaries and Coastal Seas, vol. 22 (11): 1835–56. https://doi.org/10.1016/S0278-4343(02)00041-9.